MATERIALS CHEMISTRY FRONTIERS

CHINESE CHEMICAL SOCIETY

ROYAL SOCIETY OF CHEMISTRY

RESEARCH ARTICLE

View Article Online
View Journal | View Issue

Cite this: *Mater. Chem. Front.*, 2024, **8**, 1827

Efficient quasi-2D tin perovskite solar cells based on mixed monoammonium and diammonium terminal molecules†

Zihao Zang,[a] Mingyu Ma,[a] Xianyuan Jiang,[a] Wenjia Zhou,[a] Chaowaphat Seriwattanachai,[b] Pongsakorn Kanjanaboos [b] and Zhijun Ning *[a]

Received 31st December 2023,
Accepted 15th February 2024

DOI: 10.1039/d3qm01354e

rsc.li/frontiers-materials

Tin perovskite is emerging as the most promising candidate for lead-free perovskite solar cells. However, the poor carrier transport properties, such as a short diffusion length, low carrier mobility and severe recombination, limit the boom of tin perovskite solar cells. In this work, we explored mixed monoammonium and diammonium terminal ligands to construct a quasi-2D tin perovskite film. The use of a diammonium ligand reduces the total number of terminal ligands in the film, and it retards perovskite film growth, which enhances the film orientation. These improvements enhance the carrier mobility and carrier diffusion length. As a result, the device shows enhanced current density and power conversion efficiency of 14.3%.

1 Introduction

The outstanding optoelectronic properties exhibited by tin perovskites, such as high absorption coefficients, low exciton binding energies and desirable bandgaps, render them as one of the most promising candidates for lead-free perovskites with a theoretical power conversion efficiency (PCE) of up to 33.4% based on the Shockley–Queisser equation.[1] Over the past decade, several seminal strategies have been employed to enhance the efficiency of tin perovskite solar cells (TPSCs) from approximately 6% to over 14%,[2–6] including compositional manipulation,[7–9] additive engineering,[10–13] surface modification[14,15] and device architecture design.[16–18]

The incorporation of low dimensional structures in the film plays a significant role in improving the performance of TPSCs among various methods, given its capability to effectively modulate the crystallization and reduce oxidation simultaneously.[4,5,19] The use of quasi-2D structures significantly improves the performance of tin perovskite solar cells.[20] Various linear and aromatic amines are employed as terminal molecules to form low-dimensional structures including Ruddlesden–Popper (RP) and Dion–Jacobson (DJ) phase. Based on π-conjugated terminal molecules such as fluoro-phenethylammonium and 2-phenoxyethylamine, the performance of TPSC is approaching 15%.[4,21] Alkylammonium such as butylammonium is explored as terminal ligand to enhance the device performance of TPSCs as well, with efficiency up to 12.36%.[22] Heterocyclic amines such as imidazolium are used for TPSCs as well and the efficiency is up to 12.5%.[23] These interlayers not only enhance crystal alignment and foster smoother surfaces, but also curb defects while resisting oxidation.

Recent research about the low-dimensional structure in tin perovskite films has mostly focused on RP phase constructed by double layers of insulated bulky monovalent organic cation pairs with a van der Waals gap between them.[24,25] This double layer of molecules between perovskite slabs gives a long distance resulting in a large barrier for carrier transport. As a result, suffering from deteriorated carrier transport properties, TPSCs based on RP phase low-dimensional structures show relatively small current densities ($\sim$20 mA cm^{-2} in general), which is one important factor that limits the PCE of TPSCs.[4]

Due to the high Lewis acidity of tin, it is generally difficult to control tin perovskite film growth giving rise to large defect density. The fast growth of tin perovskite film is one important factor for the high defect density of the film. The use of additives with Lewis base functional groups to manipulate perovskite film growth is an important approach to improve the film quality. By using 6-maleimidohexanehydrazide trifluoroacetate salt as an additive to passivate the defects, a champion PCE of 13.64% is achieved.[15] Similarly, 2-guanidinoacetic acid can be used to reduce Sn vacancies and raise the PCE up to 13.7%.[26] By adding ethylenediammonium dibromide additive, a champion PCE of 14.2% is achieved.[27] Although the defect density of tin perovskite film is much reduced based on these strategies, the carrier lifetime and diffusion length are still much less than those of lead perovskite

[a] *School of Physical Science and Technology, ShanghaiTech University, Shanghai, 201210, China. E-mail: ningzhj@shanghaitech.edu.cn*
[b] *School of Materials Science and Innovation, Faculty of Science, Mahidol University, Nakhon Pathom, 73170, Thailand*

† Electronic supplementary information (ESI) available. See DOI: https://doi.org/10.1039/d3qm01354e

films.[28] Consequently, regulating the tin perovskite structure and reducing defect density are still highly desirable for tin perovskite films.

In this work, we explored diammonium molecules to partly replace the phenylethylammonium (PEA) to manipulate the film structure and crystal growth kinetics. The diammonium molecules reduce the barrier for carrier transport, and they regulate the film growth kinetics. The film shows enhanced orientation and larger carrier diffusion length. The optimized device exhibits a champion efficiency of 14.3%, ranking among the highest efficiencies achieved in TPSCs.

2 Experimental section

Perovskite films were prepared by a one-step antisolvent method similar to previous work.[5] To prepare the control perovskite ($PEA_{0.2}FA_{0.8}SnI_{2.8}SCN_{0.2}$) precursor, 2-phenylethylammonium thiocyanate (PS), formamidine acetate (FAAc), NH_4I, SnF_2, and NH_4SCN in the molar ratio of 0.2 : 0.8 : 0.8 : 1 : 0.075 : 0.05 were added into SnI_2 solution with DMF and DMSO mixed solvent (v : v = 4 : 1). To prepare the optimized perovskite ($PEA_{0.18}XDA_{0.01}FA_{0.8}SnI_{2.8}SCN_{0.2}$) precursor, PS, *p*-Xylylenediammonium thiocyanate (XS_2), FAAc, NH_4I, SnF_2, and NH_4SCN in the molar ratio of 0.18 : 0.01 : 0.8 : 0.8 : 1 : 0.075 : 0.05 were added into SnI_2 solution. The precursor is stirred at room temperature overnight. More experimental details can be found in the ESI.†

3 Results and discussion

20% PS is added into the precursor to form control quasi-2D/3D structure perovskite films. In order to improve the quality of tin perovskite films, a small ratio of *p*-Xylylenediammonium thiocyanate (XS_2) is added to replace part of PS, and the fabricated

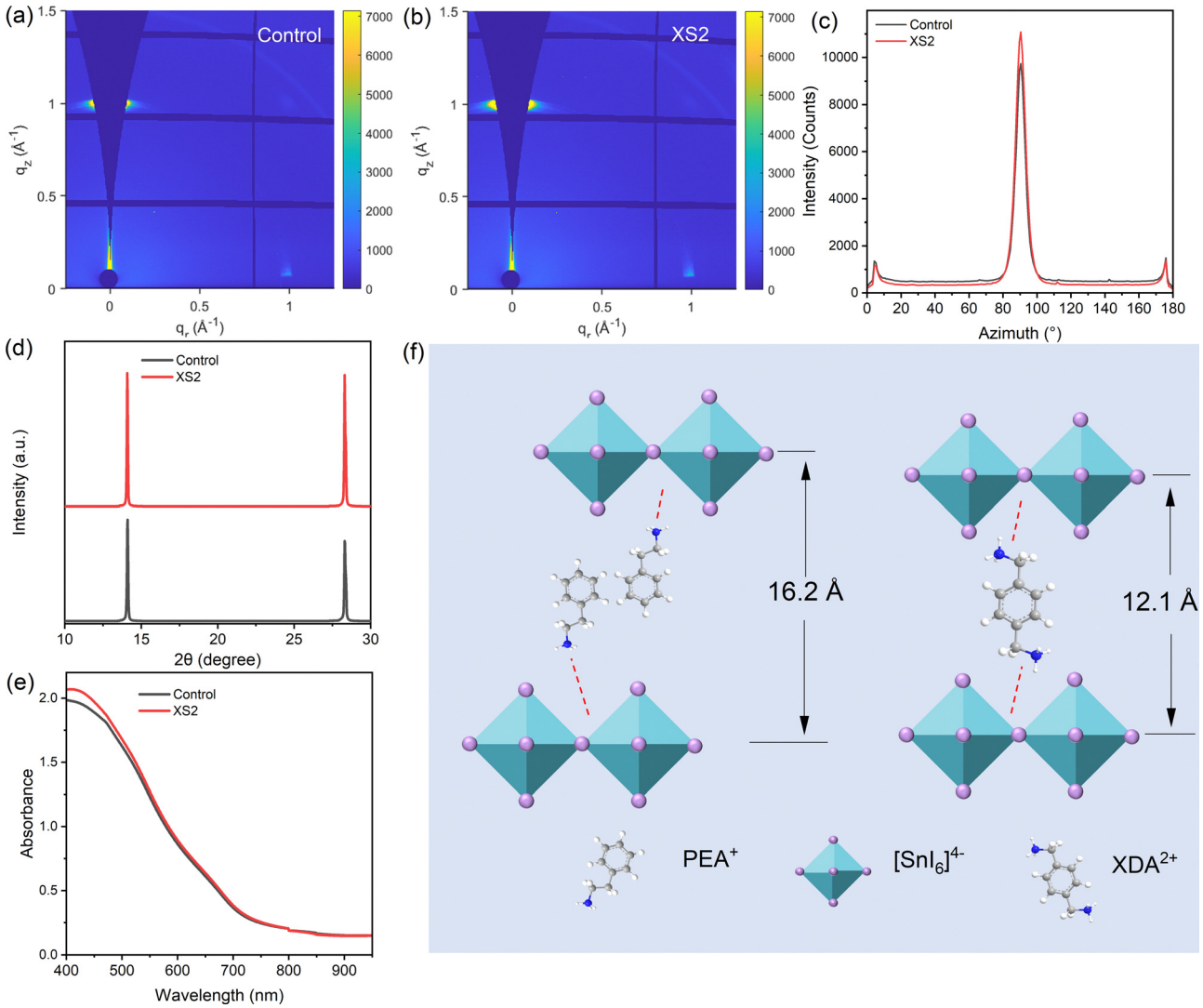

Fig. 1 Characterization of the perovskite crystal structures. (a) GIWAXS patterns of control films and (b) XS2 films with an incident angle of 0.5°. (c) GIWAXS intensity integrated azimuth at q = 1 Å^{-1}. (d) XRD patterns and (e) Abs spectra of control and XS2 films. (f) Schematic of interaction between $[SnI_6]^{4-}$ and PEA (left) or XDA (right).

film is denoted as XS2. Both films are fabricated on a PEDOT:PSS/ITO substrate with toluene as an antisolvent.

We characterized the films by grazing-incidence wide-angle X-ray scattering (GIWAXS) at an incident angle of 0.5° (Fig. 1a and b). The GIWAXS patterns of both films exhibited distinct diffraction spots of quasi-2D or 3D structures with q values of 1.00 and 1.75 $Å^{-1}$, respectively, corresponding to the (100) and (111) crystal planes.[29] Subsequently, the integration of the (100) plane diffraction intensity over the azimuthal angle was conducted numerically (Fig. 1c). While both films displayed peak diffraction signals around 90°, the XS2 film shows a stronger peak intensity, indicating a higher crystallinity in the XS2 film, which is aligned with the X-ray diffraction (XRD) patterns (Fig. 1d). Compared with the control film, the diffraction signal from the (100) plane is mainly concentrated at the azimuth angle around 90°, which means that the XS2 film is highly oriented and grows along the out-of-plane direction.[4] Fig. 1e shows the absorbance (Abs) spectra of the control and XS2 film, which have similar cut-off edges and absorbance, indicating that the structures of the two films are almost the same.

Since XS_2 has two ammonium groups, it can coordinate with two layers of $[SnI_6]^{4-}$ directly, which can reduce the distance between them. To confirm that the addition of XS_2 into the film can reduce the interlayer space, we fabricated a perovskite film with 10% XDA in the absence of PS. The film structure is characterized by GIWAXS as well (Fig. S1, ESI†). There is a clear Debye ring that can be observed at q = 0.35 $Å^{-1}$, which can be ascribed to the character signal of $XDAFASn_2X_7$.[30] Another weaker diffraction ring around q = 0.69 $Å^{-1}$ can be considered as the secondary diffraction of the former. The emergence of low-dimensional signals in $XDA_{0.1}FA_{0.8}SnX_3$ films demonstrates that XS_2 molecules can reduce the distance between the $[SnI_6]^{4-}$ layers (Fig. 1f). However, this diffraction peak is not observed for the film mixed with PS, which can be ascribed to the low concentration of XS_2.

The modification by diammonium also promotes the morphology of tin perovskite films, which is demonstrated by

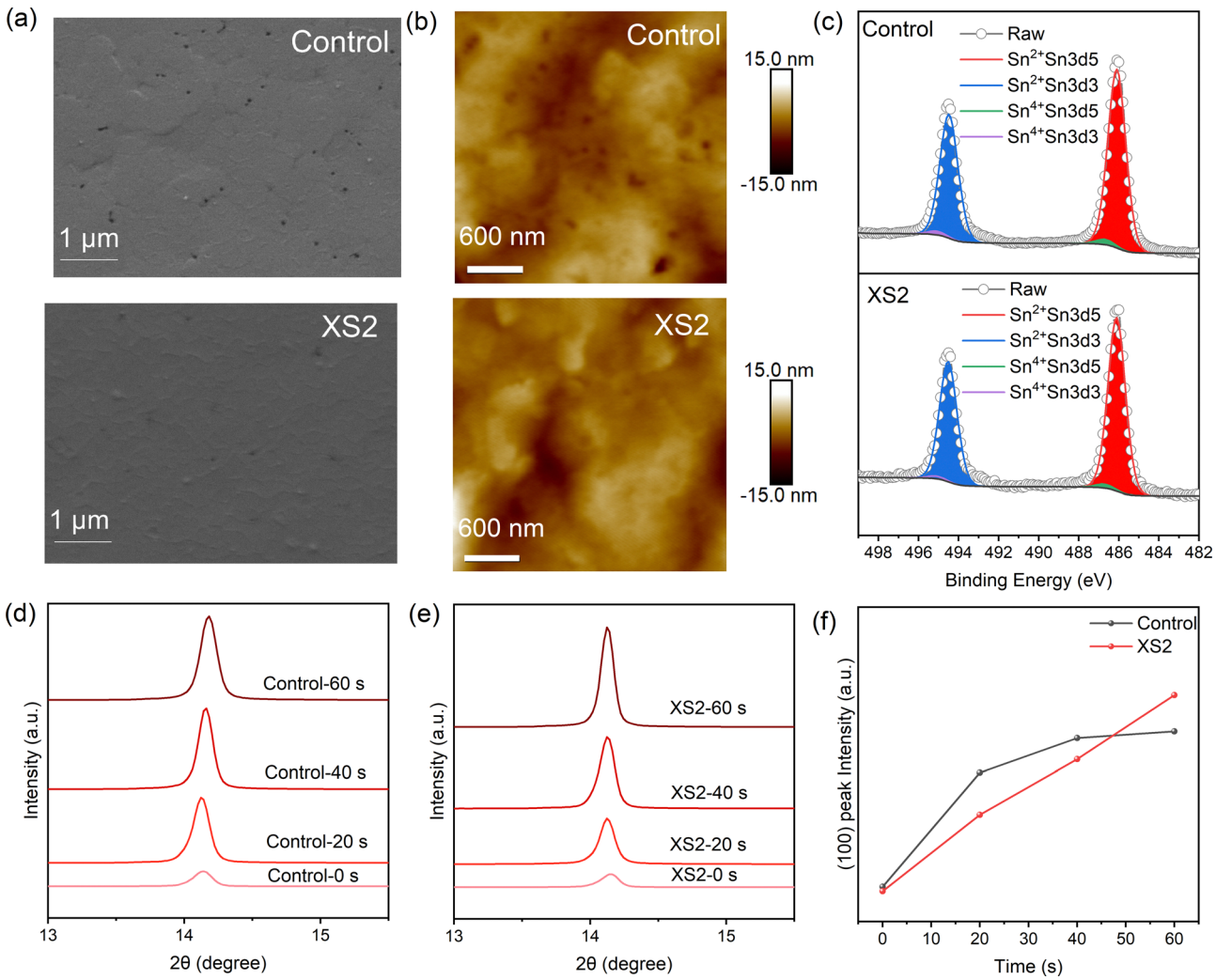

Fig. 2 Characterization of perovskite films. (a) SEM pictures of control and XS2 films. (b) AFM pictures of control and XS2 perovskite films. (c) The XPS result of the control and XS2 films. (d) The XRD patterns of the control films and XS2 films (e) based on different annealing times. (f) The (100) plane diffraction intensity of the control and XS2 perovskite thin films based on different annealing times.

scanning electron microscopy (SEM) and atomic force microscopy (AFM). As shown in Fig. 2a, although the control film seems to be smooth in general, some pinholes are contained on the surface, indicating that the quasi-2D structure does not cover the surface completely. In contrast, the XS2 film exhibits a smoother and more compact surface with reduced pinholes. AFM measurement provides accurate information about surface roughness of the two kinds of perovskite films (Fig. 2b). The R_a values are 2.1 nm and 1.9 nm for the control and XS2 films, respectively. The compact surface indicates the substantial occupation of low-dimensional structures on the surface of the films, which can shield the bulk 3D structure from the decomposing effects of oxygen and moisture. As shown in Fig. 2c, the ratio of Sn^{4+} is 2.83% in the control film, higher than that in the XS2 film (2.18%).

To identify the mechanism for the improvement in film quality, we tracked the crystal growth process during the first minute of annealing of both the control and XS2 films through X-ray diffraction (XRD) measurement (Fig. 2d–f). Before annealing, the control and XS2 films show similar intensity of the (100) plane peak, which means the crystallinity is similar. The (100) peak intensity of the control film boomed in the first 20 seconds during annealing, while the growth speed slowed down later. It can be inferred that the perovskite crystal in the control film grows rapidly at the beginning of annealing. The fast growth of tin perovskite results in increased defect density and incomplete surface coverage. However, during the first minute of XS2 film annealing, the (100) plane peak intensity shows continuous growth in 60 seconds, indicating that the crystallization rate is decreased, giving rise to high-quality perovskite films. The decelerated crystallization rate contributes to the optimized orientation and improved film morphology.

We fabricated p–i–n structured perovskite solar cells based on control and XS2 perovskite films, using the architecture of ITO/poly(3,4-ethylenedioxythiophene):poly(styrene sulfonate) (PEDOT:PSS)/tin-perovskite/indene-C_{60} bisadduct (ICBA)/bathocuproine (BCP)/Ag, as shown in the cross-sectional SEM image (Fig. 3a). Fig. 3b presents the current density–voltage (J–V) curves of the best-performing control and XS2 TPSCs measured under simulated AM 1.5 G illumination. The champion control solar cell obtains a PCE of 13.27% under reverse scan with an open-circuit voltage (V_{OC}) of 0.91 V, a short-circuit current density (J_{SC}) of 18.91 mA cm^{-2} and a fill factor (FF) of 76.65%. Due to hysteresis, the PCE under forward scan decreases to 12.84%. The champion XS2 TPSC reaches an enhanced remarkably high PCE of 14.31% with minor hysteresis, with a V_{OC} of 0.90 V, a J_{SC} of 20.70 mA cm^{-2}, and an FF of 76.96%. The external quantum efficiency (EQE) curves of both the control and XS2 devices are presented in Fig. 3c, and the J_{SC} values integrated from the EQE curves are 19.18 and 19.96 mA cm^{-2} for the control and XS2 device, respectively, matching

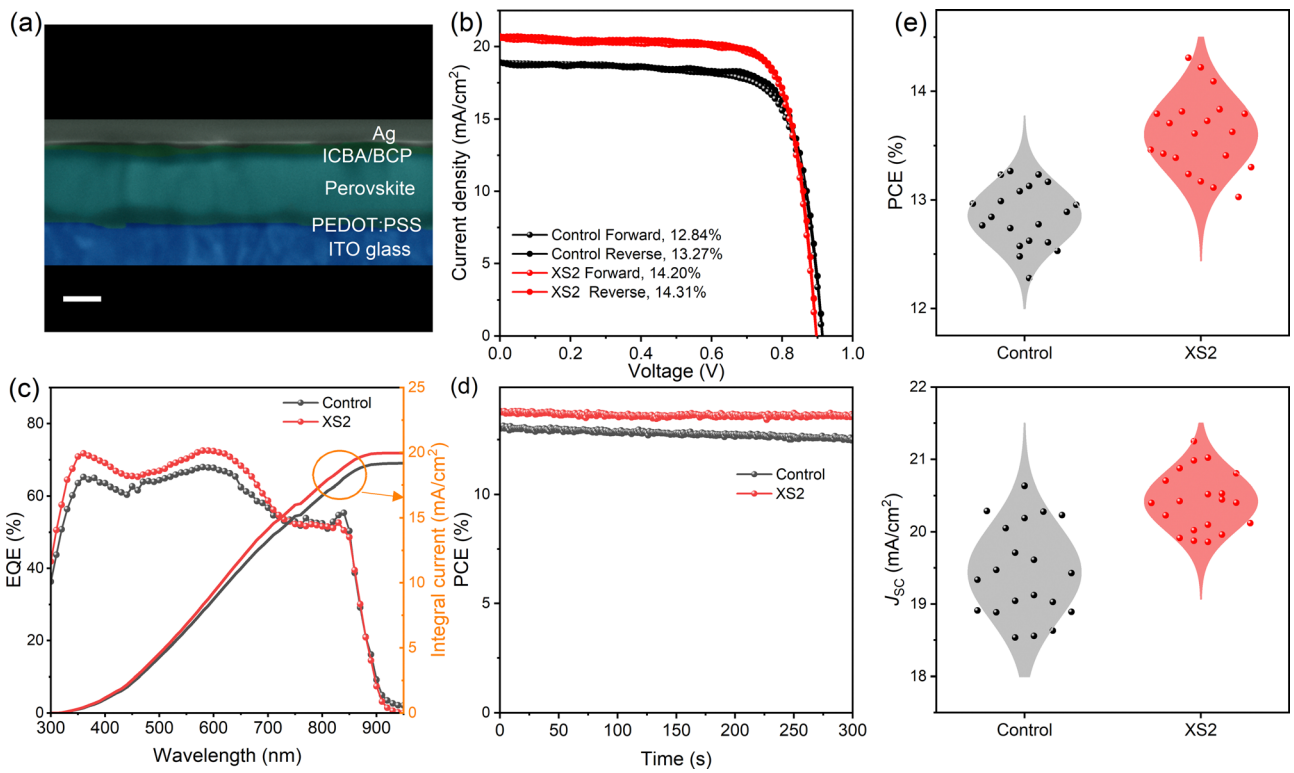

Fig. 3 Device performance. (a) A high-resolution cross-sectional SEM image of a complete device. The scale bar is 100 nm. (b) The current density–voltage characteristic curves under 100 mW cm^{-2} AM 1.5G illumination. (c) The EQE curves and integrated current density of the control and XS2 devices. (d) The maximum power point measurement for control and XS2 devices without encapsulation under simulated AM1.5 G illumination. (e) Statistical PCE and J_{SC} from 20 control and XS2 solar cells.

with the J_{SC} from the J–V curve. To show the reproducibility of XS2 in enhancing performance, a total of 20 control solar cells and 20 XS2 devices were fabricated, and their respective statistical photovoltaic parameters are presented in Table S1 (ESI†). The statistical V_{OC} and FF of two kinds of devices are almost identical (Fig. S2, ESI†), and the observed improvements in PCEs hence can be attributed to the amplified short-circuit current densities, as delineated in Fig. 3e. Specifically, the average J_{SC} of the XS2 devices measures 20.42 mA cm^{-2}, surpassing that of the control devices, which was recorded as 19.44 mA cm^{-2}. The maximum power point (MPP) measurement reveals that the XS2 device obtains an improved stability (Fig. 3d). A PCE of 13.57%, 98.3% of the initial efficiency, is maintained after 5 min of steady-state power output under 0.75 V biased voltage, while the control device maintains only 95.8% initial efficiency. Besides, the XS2 device showed increased long-term stability, maintaining ~95% of its initial efficiency after 25 days of storage in a nitrogen atmosphere, much better than that of the pristine one, which maintains only around 84% (Fig. S6, ESI†). We also fabricated devices based on tin perovskite, in which PS is replaced by XS_2 completely, and an 8.14% PCE is obtained (Fig. S3, ESI†).

To comprehensively elucidate the factors contributing to the enhanced performance of the devices, particularly the augmented J_{SC}, we tested photoluminescence (PL) spectra of the films, as shown in Fig. 4a. The PL peaks of both films are located at around 873 nm, illustrating that the small amount of XS_2 addition does not notably affect the bandgap of the tin

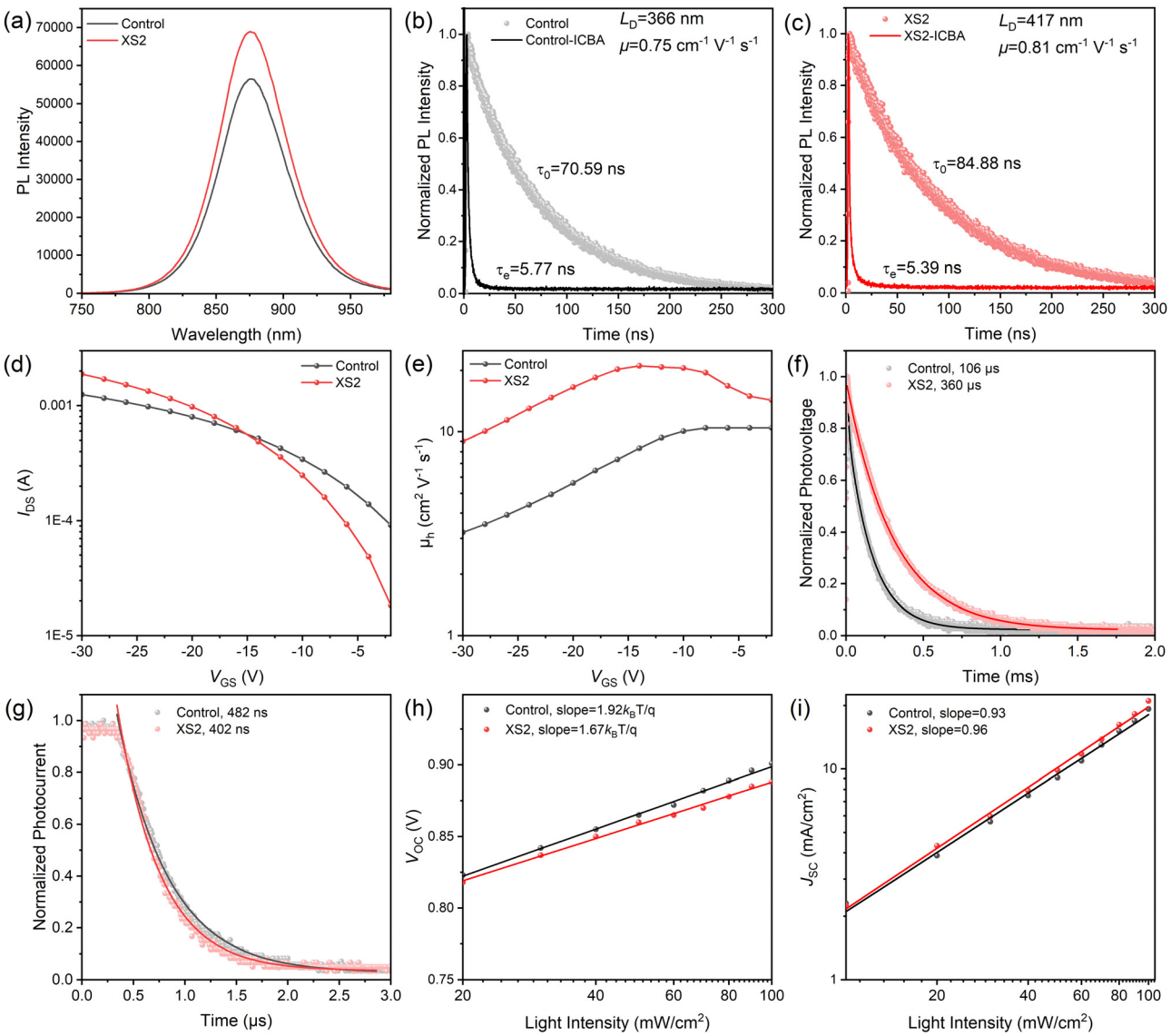

Fig. 4 Characterization of the optoelectrical properties of the devices and films. (a) PL spectra of the control and XS2 films. (b) TRPL spectra of the control and XS2 (c) films with and without ICBA, which plays a role as a quenching layer. (d) Transfer characteristics of TFTs based on the control and XS2 perovskite films. (e) Carrier mobility *versus* gate voltage (V_{GS}) curves of the control and XS2 TFTs. (f) TPV and (g) TPC for the control and XS2 encapsulated solar cells. (h) Dependence of V_{OC} and (i) J_{SC} on light intensity for the control and XS2 solar cells.

perovskite film. Nevertheless, compared to the control film, the XS2 film demonstrates higher PL intensity, suggesting the suppression of trap-assisted non-radiative recombination, which implies that the XS2 films obtain reduced defect densities.

We conducted time-resolution photoluminescence (TRPL) characterization to study the carrier dynamics. To avoid degradation stemming from oxygen and moisture, the film samples were encapsulated utilizing UV glue and glass. As delineated in Fig. 4b and c, the scatter plots demonstrate the fluorescence attenuation of both the control and XS2 perovskite films. The PL lifetimes (τ_0) of the control and XS2 films were measured as 70.59 ns and 84.88 ns, respectively, denoting an increased carrier lifetime in the XS2 device. This prolonged lifetime suggests mitigated carrier recombination and reduced defect density of the XS2 film. We then tested the PL lifetime (τ_e) of the perovskite films with an ICBA quenching layer on the surface, which is 5.77 ns and 5.36 ns for the control and XS2 device, respectively.[31] Based on the combination of τ_0 and τ_e values, the electron diffusion length and mobility of the control film are calculated to be 366 nm and 0.75 $cm^2\ V^{-1}\ s^{-1}$, respectively. For XS2 films, the calculated values are 417 nm and 0.81 $cm^2\ V^{-1}\ s^{-1}$, respectively, surpassing metrics of the control film. The extended charge diffusion length facilitates a more effective gathering of photogenerated carriers.

The improvement in carrier mobility was further corroborated by characterization of thin-film transistors (TFTs) based on control and XS2 perovskite films. The current density is improved in the negative direction, indicating p-type character of the film (Fig. 4d). The calculated carrier mobility values under varying gate voltages (V_{GS}) are outlined in Fig. 4e. The carrier mobility attained for the XS2 film reaches as high as 21.1 $cm^2\ V^{-1}\ s^{-1}$, a notable advancement compared to the control TFT's (10.4 $cm^2\ V^{-1}\ s^{-1}$). This enhancement in carrier transport dynamics can be ascribed to the modification by the diammonium molecule that reduces the thickness of the quantum well and enhances crystal orientation.

Other electrical characterizations of the devices were conducted to verify the effect of XS_2 modification on defect density. As shown in Fig. 4f, transient photovoltage (TPV) measurements reveal a prolonged charge recombination lifetime of the XS2 films (360 μs), in comparison with the control device (106 μs). This outcome validates that carriers exhibit a prolonged residence time within the target device, benefitting from a reduced density of trap states and inhibited nonradiative carrier recombination.[32] Fig. 4g shows that the transient photocurrent delay time of the XS2 device was estimated to be 402 ns, which is shorter than that of the control device (482 ns), which can be ascribed to the enhanced carrier mobility and reduced defect density.[33]

We also investigated the V_{OC} and J_{SC} of the TPSCs under light intensities varying from 20 to 100 mW cm^{-2} to further study the charge recombination. Fig. 4h represents the relationship between light intensity and V_{OC}, which can be depicted as

$$V_{OC} = \frac{nk_BT}{q}\ln\left(\frac{I}{I_0}+1\right) \quad (1)$$

where n is the ideality factor, K_B is the Boltzmann constant, T is the temperature in Kelvin, I is the light intensity, and I_0 is the initial light intensity.[34,35] The ideality factor of the optimized XS2 device is calculated as 1.67, while the corresponding value of the control device is 1.92. A decreased ideality factor demonstrates less energy loss due to less nonradiative trap-assisted Shockley–Read–Hall (SRH) recombination.[36] The light intensity dependence of J_{SC} for the XS2 device has a higher slope of 0.96 compared to 0.92 for the control device (Fig. 4i), which is consistent with the result of TPV. We also calculated the dark saturation current density (J_0) of two kinds of devices (Fig. S7, ESI†). The J_0 values of the control and XS2 devices are 8.67×10^{-8} mA cm^{-2} and 2.04×10^{-8} mA cm^{-2}, respectively, proving that the nonradiative recombination in the XS2 device is suppressed.

4 Conclusion

In summary, we explored *p*-Xylylenediammonium thiocyanate to manipulate the structure of quasi-2D tin perovskite films and improve the properties of carrier transportation. The introduction of XS_2 tunes the crystallization process and slows down the crystallization rate. As a consequence, the optimized films obtain a more compact surface, an enhanced crystal orientation and a reduced defect density. The modification of XS_2 improves the conductivity of the tin perovskite crystal, resulting in enhanced carrier mobility and prolonged carrier diffusion length, and decreased nonradiative trap-assisted recombination. As a result, a champion efficiency of 14.3% is obtained. This work provides an effective strategy to improve the quality of quasi-2D tin perovskite films by mixing double kinds of terminal ligands.

Conflicts of interest

The authors declare no competing interests.

Acknowledgements

The authors gratefully acknowledge financial support from the National Natural Science Foundation of China (92056119, 61935016, 22175118, and 22209113), the National Key Research and Development Program of China (under Grant No. 2021YFA0715502), the Science and Technology Commission of Shanghai Municipality (20XD1402500 and 20JC1415800), the China Postdoctoral Science Foundation (2021M702187), the Double First-Class Initiative Fund of ShanghaiTech University, and Centre for High-resolution Electron Microscopy (ChEM), SPST, ShanghaiTech University, under contract no. EM02161943.

References

1 X. Jiang, Z. Zang, Y. Zhou, H. Li, Q. Wei and Z. Ning, Tin Halide Perovskite Solar Cells: An Emerging Thin-Film Photovoltaic Technology, *Acc. Mater. Res.*, 2021, **2**, 210–219.

2 F. Hao, C. C. Stoumpos, D. H. Cao, R. P. H. Chang and M. G. Kanatzidis, Lead-free solid-state organic–inorganic halide perovskite solar cells, *Nat. Photonics*, 2014, **8**, 489–494.
3 J. Zhou, M. Hao, Y. Zhang, X. Ma, J. Dong, F. Lu, J. Wang, N. Wang and Y. Zhou, Chemo-thermal surface dedoping for high-performance tin perovskite solar cells, *Matter*, 2022, **5**, 683–693.
4 H. Li, Z. Zang, Q. Wei, X. Jiang, M. Ma, Z. Xing, J. Wang, D. Yu, F. Wang, W. Zhou, K. S. Wong, P. C. Y. Chow, Y. Zhou and Z. Ning, High-member low-dimensional Sn-based perovskite solar cells, *Sci. China: Chem.*, 2023, **66**, 459–465.
5 X. Jiang, Z. Zang, M. Ma, J. Wang, H. Wang and Z. Ning, Highly Efficient Tin Perovskite Solar Cells Based on a Triple Reactant Strategy, *ACS Photonics*, 2023, **10**, 1992–1998.
6 Z. Zhang, Y. Huang, C. Wang, Y. Jiang, J. Jin, J. Xu, Z. Li, Z. Su, Q. Zhou, J. Zhu, R. He, D. Hou, H. Lai, S. Ren, C. Chen, X. Gao, T. Shi, W. Hu, F. Fu, P. Gao and D. Zhao, Green-antisolvent-regulated distribution of p-type self-doping enables tin perovskite solar cells with efficiency over 14%, *Energy Environ. Sci.*, 2023, **16**, 3430–3440.
7 K. Nishimura, M. A. Kamarudin, D. Hirotani, K. Hamada, Q. Shen, S. Iikubo, T. Minemoto, K. Yoshino and S. Hayase, Lead-free tin-halide perovskite solar cells with 13% efficiency, *Nano Energy*, 2020, **74**, 104858.
8 Y. Zhang, B. Zhao, L. Liu, J. Zhou, X. Ma and N. Wang, Efficient Tin Perovskite Solar Cells *via* Suppressing Autoxidation in Inert Atmosphere, *Small*, 2023, 2306115.
9 G. Liu, X. Jiang, W. Feng, G. Yang, X. Chen, Z. Ning and W. Q. Wu, Synergic Electron and Defect Compensation Minimizes Voltage Loss in Lead-Free Perovskite Solar Cells, *Angew. Chem., Int. Ed.*, 2023, **62**, e202305551.
10 S. Wang, H. Yao, W. Zhu, C. Wu, Z. Tang, J. Liu, L. Ding and F. Hao, Stabilization of Perovskite Lattice and Suppression of Sn^{2+}/Sn^{4+} Oxidation via Formamidine Acetate for High Efficiency Tin Perovskite Solar Cells, *Adv. Funct. Mater.*, 2023, **33**, 2215041.
11 W. Zhang, Y. Cai, H. Liu, Y. Xia, J. Cui, Y. Shi, R. Chen, T. Shi and H. L. Wang, Organic-Free and Lead-Free Perovskite Solar Cells with Efficiency over 11%, *Adv. Energy Mater.*, 2022, **12**, 2202491.
12 Z. Zhu, X. Jiang, D. Yu, N. Yu, Z. Ning and Q. Mi, Smooth and Compact FASnI3 Films for Lead-Free Perovskite Solar Cells with over 14% Efficiency, *ACS Energy Lett.*, 2022, **7**, 2079–2083.
13 T. Li, Z. Zhang, F. He, L. Deng, Y. Yang, X. Mo, Y. Zhan and J. Liang, Alleviating the Crystallization Dynamics and Suppressing the Oxidation Process for Tin-Based Perovskite Solar Cells with Fill Factors Exceeding 80 Percent, *Adv. Funct. Mater.*, 2023, **33**, 2308457.
14 Z. Zhang, M. A. Kamarudin, A. K. Baranwal, G. Kapil, S. R. Sahamir, Y. Sanehira, M. Chen, L. Wang, Q. Shen and S. Hayase, Sequential Passivation for Lead-Free Tin Perovskite Solar Cells with High Efficiency, *Angew. Chem., Int. Ed.*, 2022, **61**, e202210101.
15 H. Li, B. Chang, L. Wang, Z. Wang, L. Pan, Y. Wu, Z. Liu and L. Yin, Surface Reconstruction for Tin-Based Perovskite Solar Cells, *ACS Energy Lett.*, 2022, **7**, 3889–3899.
16 B. Li, X. Wu, H. Zhang, S. Zhang, Z. Li, D. Gao, C. Zhang, M. Chen, S. Xiao, A. K. Y. Jen, S. Yang and Z. Zhu, Efficient and Stable Tin Perovskite Solar Cells by Pyridine-Functionalized Fullerene with Reduced Interfacial Energy Loss, *Adv. Funct. Mater.*, 2022, **32**, 2205870.
17 R. Balasaravanan, C. H. Kuan, S. M. Hsu, E. C. Chang, Y. C. Chen, Y. T. Tsai, M. L. Jhou, S. L. Yau, C. L. Liu, M. C. Chen and E. W. G. Diau, Triphenylamine (TPA)-Functionalized Structural Isomeric Polythiophenes as Dopant Free Hole-Transporting Materials for Tin Perovskite Solar Cells, *Adv. Energy Mater.*, 2023, **13**, 2302047.
18 T. Li, F. He, J. Liang and Y. Qi, Functional layers in efficient and stable inverted tin-based perovskite solar cells, *Joule*, 2023, **7**, 1966–1991.
19 J. Wang, C. Yang, H. Chen, M. Lv, T. Liu, H. Chen, D.-J. Xue, J.-S. Hu, L. Han, S. Yang and X. Meng, Oriented Attachment of Tin Halide Perovskites for Photovoltaic Applications, *ACS Energy Lett.*, 2023, **8**, 1590–1596.
20 H. Zhu, J. Ma, P. Li, S. Zang, Y. Zhang and Y. Song, Low-dimensional Sn-based perovskites: Evolution and future prospects of solar cells, *Chemistry*, 2022, **8**, 2939–2960.
21 B. B. Yu, Z. Chen, Y. Zhu, Y. Wang, B. Han, G. Chen, X. Zhang, Z. Du and Z. He, Heterogeneous 2D/3D Tin-Halides Perovskite Solar Cells with Certified Conversion Efficiency Breaking 14%, *Adv. Mater.*, 2021, **33**, 2102055.
22 Y. Lei, Y. Li, C. Lu, Q. Yan, Y. Wu, F. Babbe, H. Gong, S. Zhang, J. Zhou, R. Wang, R. Zhang, Y. Chen, H. Tsai, Y. Gu, H. Hu, Y.-H. Lo, W. Nie, T. Lee, J. Luo, K. Yang, K.-I. Jang and S. Xu, Perovskite superlattices with efficient carrier dynamics, *Nature*, 2022, **608**, 317–323.
23 C.-H. Kuan, J.-M. Chih, Y.-C. Chen, B.-H. Liu, C.-H. Wang, C.-H. Hou, J.-J. Shyue and E. W.-G. Diau, Additive Engineering with Triple Cations and Bifunctional Sulfamic Acid for Tin Perovskite Solar Cells Attaining a PCE Value of 12.5% without Hysteresis, *ACS Energy Lett.*, 2022, **7**, 4436–4442.
24 Z. Shi, Z. Ni and J. Huang, Direct Observation of Fast Carriers Transport along Out-of-Plane Direction in a Dion–Jacobson Layered Perovskite, *ACS Energy Lett.*, 2022, **7**, 984–987.
25 M. Liu and T. Pauporté, Additive Engineering for Stable and Efficient Dion–Jacobson Phase Perovskite Solar Cells, *Nano-Micro Lett.*, 2023, **15**, 134.
26 G. Liu, Y. Zhong, W. Feng, M. Yang, G. Yang, J. X. Zhong, T. Tian, J. B. Luo, J. Tao, S. Yang, X. D. Wang, L. Tan, Y. Chen and W. Q. Wu, Multidentate Chelation Heals Structural Imperfections for Minimized Recombination Loss in Lead-Free Perovskite Solar Cells, *Angew. Chem., Int. Ed.*, 2022, **61**, 202209464.
27 Y. Jiang, Z. Lu, S. Zou, H. Lai, Z. Zhang, J. Luo, Y. Huang, R. He, J. Jin, Z. Yi, Y. Luo, W. Wang, C. Wang, X. Hao, C. Chen, X. Wang, Y. Wang, S. Ren, T. Shi, F. Fu and D. Zhao, Dual-site passivation of tin-related defects enabling efficient lead-free tin perovskite solar cells, *Nano Energy*, 2022, **103**, 107818.
28 Y. Chen, Z. Wang, Y. Wei, Y. Liu and M. Hong, Exciton Localization for Highly Luminescent Two-Dimensional

Tin-Based Hybrid Perovskites through Tin Vacancy Tuning, *Angew. Chem., Int. Ed.*, 2023, **62**, e202301684.

29 S. Kahmann, O. Nazarenko, S. Shao, O. Hordiichuk, M. Kepenekian, J. Even, M. V. Kovalenko, G. R. Blake and M. A. Loi, Negative Thermal Quenching in $FASnI_3$ Perovskite Single Crystals and Thin Films, *ACS Energy Lett.*, 2020, **5**, 2512–2519.

30 H. Shi, L. Zhang, H. Huang, Y. Ou, X. Wang, Z. Li, D. Chi and S. Huang, Additive Engineering for High-Performance Two-Dimensional Dion–Jacobson Pb–Sn Alloyed Perovskite Solar Cells, *Energy Technol.*, 2022, **10**, 2200983.

31 G. Xing, N. Mathews, S. Sun, S. S. Lim, Y. M. Lam, M. Grätzel, S. Mhaisalkar and T. C. Sum, Long-Range Balanced Electron- and Hole-Transport Lengths in Organic-Inorganic $CH_3NH_3PbI_3$, *Science*, 2013, **342**, 344–347.

32 D. Cui, X. Liu, T. Wu, X. Lin, X. Luo, Y. Wu, H. Segawa, X. Yang, Y. Zhang, Y. Wang and L. Han, Making Room for Growing Oriented $FASnI_3$ with Large Grains via Cold Precursor Solution, *Adv. Funct. Mater.*, 2021, **31**, 2100931.

33 Z. Cao, S. Wang, W. Zhu, L. Ding and F. Hao, Minimizing the Voltage Deficit of Tin Halide Perovskite Solar Cells with Hydroxyurea-Doped PEDOT:PSS, *Sol. RRL*, 2022, **7**, 2200889.

34 S. Zou, S. Ren, Y. Jiang, Y. Huang, W. Wang, C. Wang, C. Chen, X. Hao, L. Wu, J. Zhang and D. Zhao, Efficient Environment-friendly Lead-free Tin Perovskite Solar Cells Enabled by Incorporating 4-Fluorobenzylammonium Iodide Additives, *Energy Environ. Mater.*, 2023, **6**, e12465.

35 Q. Jiang, Y. Zhao, X. Zhang, X. Yang, Y. Chen, Z. Chu, Q. Ye, X. Li, Z. Yin and J. You, Surface passivation of perovskite film for efficient solar cells, *Nat. Photonics*, 2019, **13**, 460–466.

36 Z. Yu, J. Wang, B. Chen, M. A. Uddin, Z. Ni, G. Yang and J. Huang, Solution-Processed Ternary Tin (II) Alloy as Hole-Transport Layer of Sn–Pb Perovskite Solar Cells for Enhanced Efficiency and Stability, *Adv. Mater.*, 2022, **34**, 2205769.

